Field-Induced Paramagnons at the Metamagnetic Transition of $Ca_{1.8}Sr_{0.2}RuO_4$

P. Steffens,[1] Y. Sidis,[2] P. Link,[3,*] K. Schmalzl,[4] S. Nakatsuji,[5] Y. Maeno,[6] and M. Braden[1]

[1]*II. Physikalisches Institut, Universität zu Köln, Zülpicher Strasse 77, D-50937 Köln, Germany*
[2]*Laboratoire Léon Brillouin, C.E.A./C.N.R.S., F-91191 Gif-sur-Yvette CEDEX, France*
[3]*Forschungsneutronenquelle Heinz Maier-Leibnitz (FRM-II), TU München, Lichtenbergstrasse 1, 85747 Garching, Germany*
[4]*Juelich Centre for Neutron Science, Forschungszentrum Juelich, Outstation ILL, 38042 Grenoble, France*
[5]*Institute for Solid State Physics, University of Tokyo, Kashiwa, Chiba 277-8581, Japan*
[6]*Department of Physics, Kyoto University, Kyoto 606-8502, Japan*

(Received 30 March 2007; published 19 November 2007; corrected 21 November 2007)

The magnetic excitations in $Ca_{1.8}Sr_{0.2}RuO_4$ were studied across the metamagnetic transition and as a function of temperature using inelastic neutron scattering. At low temperature and low magnetic field the magnetic response is dominated by a complex superposition of incommensurate antiferromagnetic fluctuations. Upon increasing the magnetic field across the metamagnetic transition, paramagnon and finally well-defined magnon scattering is induced, partially suppressing the incommensurate signals. The high-field phase in $Ca_{1.8}Sr_{0.2}RuO_4$, therefore, has to be considered as an intrinsically ferromagnetic state stabilized by the magnetic field.

DOI: 10.1103/PhysRevLett.99.217402 PACS numbers: 78.70.Nx, 74.70.Pq, 75.40.Gb

Metamagnetic (MM) transitions have recently attracted considerable interest as, despite their typically first order character, a quantum phase transition can be realized when the critical end point is driven to zero temperature. By varying the direction of the applied field, this suppression of the critical end point can be achieved in the double-layer ruthenate $Sr_3Ru_2O_7$ inducing fascinating quantum-critical phenomena [1].

$Ca_{1.8}Sr_{0.2}RuO_4$ belongs to the single-layered ruthenates but exhibits a MM transition very similar to that in $Sr_3Ru_2O_7$. $Ca_{1.8}Sr_{0.2}RuO_4$ is a metal on the border of the transition into the Mott-insulating state [2]. The very high electronic specific-heat coefficient in the range of values in typical heavy-fermion compounds indicates strong magnetic fluctuations [3]. At magnetic fields of 2–8 T (depending on the field orientation) $Ca_{1.8}Sr_{0.2}RuO_4$ undergoes the MM transition into a state with high magnetic polarization of about $0.7\mu_B$ per Ru [3] accompanied by a shift in the occupation of the Ru $4d$ t_{2g} states [4,5]. However, it is still an open issue whether the high-field phase is intrinsically ferromagnetic (FM) or just polarized, in $Ca_{1.8}Sr_{0.2}RuO_4$ as well as in $Sr_3Ru_2O_7$. The MM transition in $Ca_{1.8}Sr_{0.2}RuO_4$ is smeared out due to the intrinsic disorder caused by the chemical doping. As a consequence, any quantum-critical scaling might be strongly modified [6]. However, the simpler crystal structure with only one RuO_2 layer and the resulting simpler (essentially two-dimensional) electronic band structure render $Ca_{1.8}Sr_{0.2}RuO_4$ more favorable for an analysis of the underlying mechanism. Previous studies on related ruthenates, $Ca_{2-x}Sr_xRuO_4$ with $x = 0.62$ [7] and $Sr_3Ru_2O_7$ [8,9], have revealed the complexity of the magnetic response at zero field but did not address the MM transition.

The cross section for magnetic inelastic neutron scattering is given by the imaginary part of the susceptibility $\chi''(\mathbf{Q}, \omega)$ [10]:

$$\frac{d^2\sigma}{d\Omega d\omega} \propto \frac{F^2(\mathbf{Q})}{1 - \exp(-\frac{\hbar\omega}{k_B T})} \chi''(\mathbf{Q}, \omega).$$

$F(\mathbf{Q})$ is the magnetic form factor. We used two coaligned single crystals of $Ca_{1.8}Sr_{0.2}RuO_4$ of about 3 mm diameter and 15 mm length each, grown at Kyoto University. The measurements were performed on different neutron triple-axis spectrometers: 2 T and 4 F at the LLB, Saclay, IN22 at the ILL, Grenoble, and PANDA at FRM-II, Garching. On the latter two we applied magnetic fields up to 10 T using vertical cryomagnets, i.e., perpendicular to the scattering plane. Two different sample orientations were used: one with the a and the b axis, and one with the a and the c axis in the scattering plane. Throughout this Letter, we use the pseudotetragonal notation $a = b = 3.76$ Å and $c = 12.55$ Å in accordance with the majority of the literature, neglecting the structural distortions [11]. The sample was twinned, with approximately equal amounts of both orthorhombic twins.

Let us first consider the spin dynamics in $Ca_{1.8}Sr_{0.2}RuO_4$ at zero magnetic field and low temperature, $T = 2$ K. Figure 1 shows the neutron intensity at constant energy transfer of $\hbar\omega = 2.5$ meV mapped out in reciprocal space around $\mathbf{Q} = (1, 0, 0)$. For the description of the magnetism we restrict ourselves on the two dimensions formed by the RuO_2 plane (ab plane), because the correlation of adjacent planes, i.e., along the c axis, is negligible [7,12]. Therefore, $\mathbf{Q} = (1, 0, 0)$ can be regarded as a FM zone center, and the area shown in Fig. 1 covers already a full Brillouin zone. The magnetic scattering is broadly distributed around the FM zone center resembling that observed in $Ca_{1.38}Sr_{0.62}RuO_4$ [7], where the MM transition is strongly suppressed. At the temperature of 2 K in $Ca_{1.8}Sr_{0.2}RuO_4$,

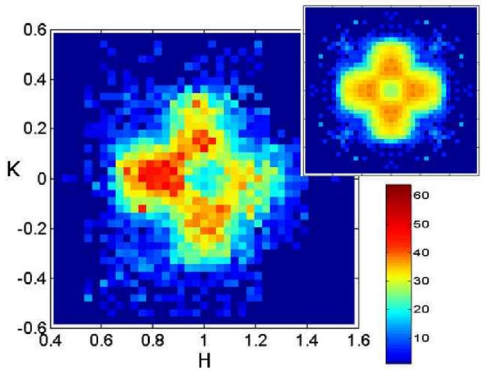

FIG. 1 (color online). Mapping of the magnetic intensity in the a^*/b^* plane of reciprocal space around $\mathbf{Q} = (1, 0, 0)$. Data are taken at $T = 2$ K and at an energy transfer of 2.5 meV. A smooth background is subtracted. The inset shows the same data, but fully symmetrized and corrected for the magnetic form factor $F(\mathbf{Q})$.

we always find a minimum at the FM center $(1, 0, 0)$ in cuts along the [100] or [110] directions [Figs. 1, 2(a), and 2(b)]. Furthermore, the data cannot be described by a single contribution centered on the a^* or b^* axes; the scans along [010] show steep edges at $\mathbf{Q} = (1, \pm 0.35, 0)$ and a relatively broad and flat plateau between $(1, \pm 0.1, 0)$ and $(1, \pm 0.3, 0)$. For a phenomenological description, we fit the magnetic scattering by *two* Gaussian contributions on each side of $(1, 0, 0)$ with approximately equal intensity and width. These contributions are centered at $\mathbf{q}_1 = (1, 0.12 \pm 0.01, 0)$ and $\mathbf{q}_2 = (1, 0.27 \pm 0.01, 0)$ and the

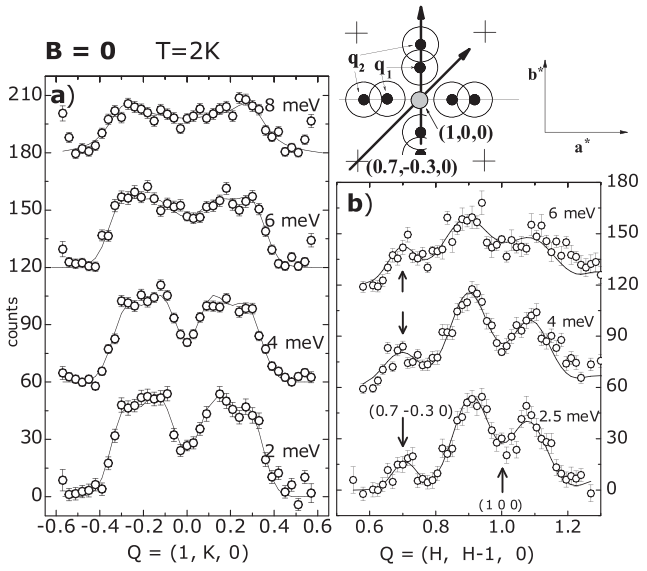

FIG. 2. Constant energy scans: (a) along b^*, (b) along the diagonal of the Brillouin zone. The sketch on top illustrates the positions of the incommensurate magnetic signals as described in the text, and the bold arrows are the trajectories of the scans in reciprocal space. The crosses are the weaker α/β nesting signal at $(1, 0, 0) + (\pm 0.3, \pm 0.3, 0)$. The lines are fits with Gaussians centered at the positions shown in the sketch.

equivalent positions in pseudotetragonal symmetry. We may exclude that the inner signal stems from an isotropic paramagnon signal, as there is no evidence for a ring of scattering in Fig. 1 and as the intensity does not show the expected increase [10] when approaching $(1, 0, 0)$ and low energies. There is no visible shift of the $\mathbf{q}_1$, $\mathbf{q}_2$ signals as a function of energy, but rather a broadening that finally suppresses the minimum at the center. In agreement with the study on $Ca_{1.38}Sr_{0.62}RuO_4$ [7], the $\mathbf{q}_1$, $\mathbf{q}_2$ fluctuations exhibit a characteristic energy of 2.7 ± 0.2 meV. From the analysis of the geometrical factor at different equivalent $\mathbf{Q}$ points, we deduce that for these fluctuations χ_c'' is significantly smaller than χ_{ab}'', which is opposite to the finding in Sr_2RuO_4 [13].

In the layered ruthenates, the Fermi surface consists of several sheets related with the three t_{2g} states of the Ru $4d$ shell [14]: two sheets arise from nearly one-dimensional bands of $d_{xz/yz}$ character, named α and β, and the γ sheet originates from the two-dimensional $4d_{xy}$ band. We assume that the $\mathbf{q}_1$, $\mathbf{q}_2$ signals arise from the γ band, since this band has been shown to carry the magnetization in $Ca_{1.5}Sr_{0.5}RuO_4$ [15], although its topology (electronlike or holelike [16]) in the structurally distorted compound is not fully established yet.

The magnetic excitations described above strongly resemble those observed in $Sr_3Ru_2O_7$ with two incommensurate contributions on the a^* or b^* axes at almost the same positions ($x = 0.09$ and 0.25) [8]. This remarkable agreement suggests that magnetic properties and, in particular, the MM mechanism should be very similar in these ruthenates.

The diagonal scans in Fig. 2(b) show a weaker signal at $\mathbf{Q}_{(\alpha\beta)} \approx (0.7, -0.3, 0)$, at the position where the dominant magnetic fluctuations occur in Sr_3RuO_4 due to nesting in the α and β Fermi-surface sheets [12,14]. The structural distortions in $Ca_{1.8}Sr_{0.2}RuO_4$ cause a folding of the electronic bands with respect to $(0.5, 0.5, 0)$ implying a complex Fermi surface as well as a complex Lindhard function. However, the strong nesting tendency observed in Sr_2RuO_4 should be rather robust and can be taken as a rough estimate of the band filling. In $Ca_{1.8}Sr_{0.2}RuO_4$ the filling of the α, β bands seems thus to be similar to that in Sr_2RuO_4, clearly contradicting the proposal of an orbital-selective Mott transition [17] requiring a significant redistribution of orbital occupation.

Upon heating to intermediate temperatures of the order of 10 K, the magnetic response changes significantly, developing strong paramagnon scattering of truly FM character on top of the already complex low-temperature antiferromagnetic (AFM) response described above. Upon cooling, the paramagnon contribution appears below $\sim$50 K, passes a maximum, and becomes suppressed at the lowest temperatures; see Fig. 3. The paramagnon scattering exhibits a significantly smaller characteristic energy of the order of 0.2–0.6 meV, which strongly depends on temperature. Via calibration by an acoustic phonon, we

may determine $\chi''(Q, \omega)$ in absolute units, as shown in Fig. 3, which then allows us to calculate $\chi'(Q, 0)$ by Kramers-Kronig analysis. For a single relaxor $\chi''(Q, \omega) = \frac{\chi'(Q,0)\cdot\Gamma\cdot\omega}{\Gamma^2+\omega^2}$, $\chi'(Q, 0)$ amounts to twice the maximum of the imaginary part (at $\omega = \Gamma$). $\chi''(Q_{\mathrm{FM}}, \omega)$ consists of two contributions due to the strong in-plane anisotropy, and the average $\chi''(Q_{\mathrm{FM}}, 0.4\ \mathrm{meV}) + \chi''(Q_{\mathrm{FM}}, 1\ \mathrm{meV})$ is a reasonable estimate for $\chi'(Q_{\mathrm{FM}}, 0)$. Figure 3(c) compares this estimate with the susceptibility measured by a macroscopic method yielding good agreement. The incipient FM instability in $Ca_{1.8}Sr_{0.2}RuO_4$, which due to the orbital rearrangement [4–6] is suppressed at low temperature, is thus carried by the paramagnon fluctuations.

Let us now focus on the effect of a magnetic field. The MM transition in $Ca_{1.8}Sr_{0.2}RuO_4$ occurs approximately at 6 T for a magnetic field along the c direction and at 3 T for $B \parallel a, b$ [3,5]. The even stronger in-plane anisotropy between the two orthorhombic axes (diagonals in our notation) is not relevant in our experimental geometry with B parallel to [010]; see Fig. 4. There is a drastic change at the MM transition field ($B_{\mathrm{MM}} \approx 3$ T), which corresponds to an only low-energy scale $g\mu_B B \approx 0.17$ meV: below the transition, we observe the incommensurate AFM fluctuations. Above, the response is dominated by a broad paramagnon signal around the 2D FM zone center (0, 0, 1.6). The data can be described in a very simple model of two contributions: an AFM one (taken to have always the same shape as at $B = 0$) and a FM one. It is clearly seen that the fundamental change takes place between 2 and 4 T, i.e., at the MM transition. A small AFM contribution persists to higher fields getting fully suppressed only far above the transition. The energy scans at the FM zone center,

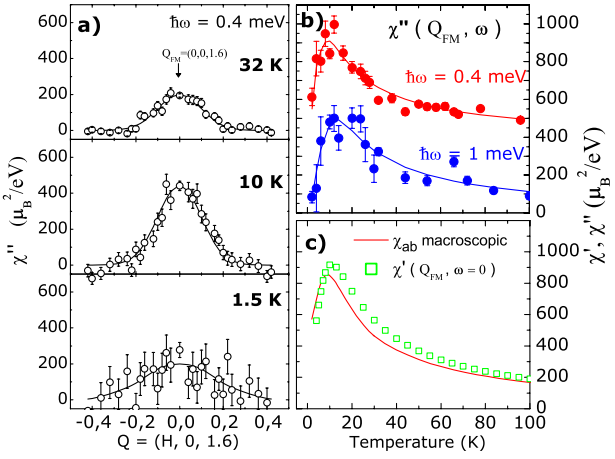

FIG. 3 (color online). Temperature dependence of the paramagnon scattering. (a) Constant energy scans at three different temperatures. In (b) we plot the intensity of the (2D) zone center $Q_{\mathrm{FM}} = (0, 0, 1.6)$ as a function of temperature for 0.4 and 1 meV energy transfer (lines are guides to the eye, 0.4 meV data shifted by $400\frac{\mu_B^2}{\mathrm{eV}}$). From the smoothed curves in (b) we estimate the real part of the susceptibility at $\omega = 0$ (see text), which is plotted in (c) together with the macroscopic susceptibility (in-plane average) from Ref. [2].

Fig. 4(c), confirm that upon applying a magnetic field the FM response is enhanced and that its spectral weight shifts to higher energies at fields above the transition. The transition is further seen in the field dependence of the intensity at fixed energy [Fig. 4(d) and 4(e)]. Low-energy paramagnon fluctuations seem to govern the thermodynamics of the MM transition. Their enhancement at the critical field shown in Fig. 4(e) may explain the observation that the electronic specific heat passes a maximum at the transition [18], because the low-energy magnetic fluctuations give a large contribution to the electronic specific heat; see also Ref. [7].

The quantitative analysis of the paramagnon signal in the $B \parallel [010]$ configuration is difficult. Because of the low vertical resolution of the focusing spectrometer, the dispersion along b^* is averaged. Furthermore, the measured susceptibility consists of a superposition of several components. At $\mathbf{Q} = (0, 0, L)$ we measure the sum of the in-plane components χ''_{ab}. Because the field is along b^*, χ''_{ab} splits into two components, $\chi^{\parallel}$ and $\chi^{\perp}$, parallel and transverse to the applied field. The transverse susceptibility is associated with electronic spin-flip processes. Therefore, a

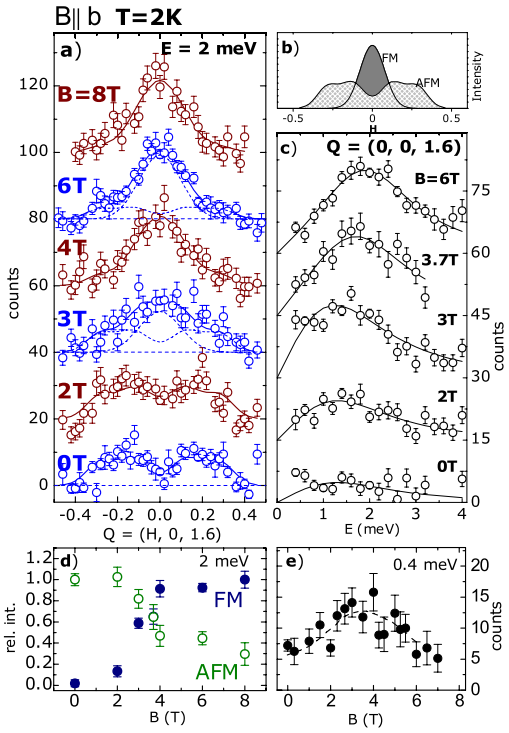

FIG. 4 (color online). Magnetic scattering for magnetic fields applied along the b axis: (a) Constant energy scans along [100]. Lines assume a superposition of an AFM and a FM contribution [the latter centered at $Q_{\mathrm{FM}} = (0, 0, 1.6)$], a sketch of these contributions is drawn in (b). (c) Energy scans at the FM position Q_{FM}. The intensities of the FM and AFM contributions fitted to the scans in (a) relative to their values at 0 and 8 T, respectively, are shown in (d) as a function of the field. (e) The field dependence of the low-energy part at Q_{FM}. [Lines in (c) and (e) are guides to the eye.]

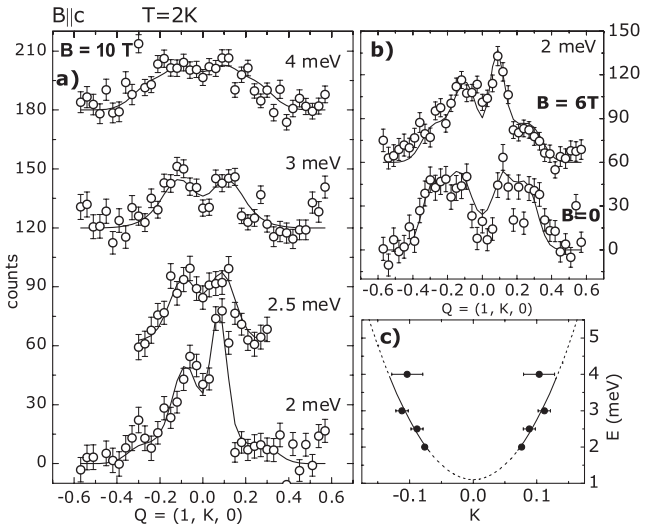

FIG. 5. (a) Constant energy scans above the MM transition ($B = 10$ T, $B \parallel c$) in the same configuration as the scans in Fig. 2. The lines are fits consisting of two contributions: the AFM one was taken to be the same as in Fig. 2(a) times a variable scale factor ≤ 1; the magnon was added as two Gaussians at symmetric positions, but variable width to account for focusing effects of the spectrometer. In (b) the 2 meV scans at 0 and 6 T are compared. In (c), the fitted peak positions are plotted together with a parabolic dispersion.

Zeeman-type energy gap, $g\mu_B B \approx 1$ meV for a field of 10 T, superposes the spin-orbit coupling induced anisotropy gap for the transverse channel $\chi^{\perp}$, whereas $\chi^{\parallel}$ exhibits only an anisotropy gap.

The quantitative analysis is simpler when the field is applied along the c axis; see Fig. 5. The low vertical resolution then averages along c^*, where the magnetic dispersion is negligible. Again there is a drastic change at the MM transition ($B_{\mathrm{MM}} = 6$ T); see Figs. 5(a) and 5(b) and the zero field data taken under the same conditions in Fig. 2. At 10 T, there is clear evidence for a well-defined magnon mode. This mode disperses outwards from $(1, 0, 0)$, rapidly broadens, and dies away with increasing frequency. It can be described by a quadratic dispersion [Fig. 5(c)] similar to a conventional ferromagnet: $\hbar\omega = g\mu_B B_{\mathrm{eff}} + Dq^2$ with a stiffness constant of 60 meV Å^2. Since the external field superposes the anisotropy terms, an effective field enters the dispersion relation. Assuming that the single-ion anisotropies nearly average out in this geometry, we set $B_{\mathrm{eff}} \approx B_{\mathrm{external}}$. The dispersion of the magnon unambiguously proves that the high-magnetization phase does not only arise from the magnetic polarization of the spins, but has to be considered as a true FM state with an intrinsic FM interaction stabilized by the magnetic field. In contrast, the FM correlation seems to be suppressed in the low-temperature low-field phase due to the orbital effects [4,5].

We mention that an enhancement of magnetic scattering near FM q vectors has also been observed in the MM transition in the heavy-fermion compound $CeRu_2Si_2$ [19], but a well-defined magnon mode has not been established in any MM transition so far.

In conclusion, our results indicate that a magnetic field corresponding to low electronic energy scales causes a fundamental change of the magnetic correlations in $Ca_{1.8}Sr_{0.2}RuO_4$. Below the MM transition, the interactions are AFM with several incommensurate scattering contributions. In particular, there is a weak signal near $(0.3, 0.3, q_L)$, i.e., very close to the position of the dominant nesting signal in Sr_2RuO_4. Magnetic correlations in $Ca_{1.8}Sr_{0.2}RuO_4$ fundamentally change upon an increase of either temperature or magnetic field. In both cases we find strong paramagnon scattering. In the high-magnetization phase we even find a well-defined magnon mode corroborating the dominance of the FM interaction and the intrinsic FM character of the high-field state.

The paramagnon fluctuations should govern the thermodynamics in $Ca_{1.8}Sr_{0.2}RuO_4$ close to its MM quantum-critical point and further document that layered ruthenates in general may exhibit an intrinsic FM instability—possibly an important ingredient to understand superconductivity in Sr_2RuO_4.

The work at Universität zu Köln was supported by the Deutsche Forschungsgemeinschaft through the Sonderforschungsbereich No. 608.

*Also at Spektrometer PANDA, Institut für Festkörperphysik, TU Dresden, Dresden, Germany.

[1] S. A. Grigera *et al.*, Science **294**, 329 (2001); R. S. Perry *et al.*, Phys. Rev. Lett. **86**, 2661 (2001); S. A. Grigera *et al.*, Science **306**, 1154 (2004).
[2] S. Nakatsuji and Y. Maeno, Phys. Rev. Lett. **84**, 2666 (2000); Phys. Rev. B **62**, 6458 (2000).
[3] S. Nakatsuji *et al.*, Phys. Rev. Lett. **90**, 137202 (2003).
[4] M. Kriener *et al.*, Phys. Rev. Lett. **95**, 267403 (2005).
[5] L. Balicas *et al.*, Phys. Rev. Lett. **95**, 196407 (2005).
[6] J. Baier *et al.*, J. Low Temp. Phys. **147**, 405 (2007).
[7] O. Friedt *et al.*, Phys. Rev. Lett. **93**, 147404 (2004).
[8] L. Capogna *et al.*, Phys. Rev. B **67**, 012504 (2003).
[9] M. B. Stone *et al.*, Phys. Rev. B **73**, 174426 (2006).
[10] See, for instance, S. W. Lovesey, *Theory of Neutron Scattering from Condensed Matter* (Clarendon, Oxford, 1984), Vol. 2; T. Moriya, *Spin Fluctuations in Itinerant Electron Magnetism* (Springer, New York, 1985).
[11] O. Friedt *et al.*, Phys. Rev. B **63**, 174432 (2001).
[12] Y. Sidis *et al.*, Phys. Rev. Lett. **83**, 3320 (1999); M. Braden *et al.*, Phys. Rev. B **66**, 064522 (2002).
[13] M. Braden *et al.*, Phys. Rev. Lett. **92**, 097402 (2004).
[14] C. Bergemann *et al.*, Adv. Phys. **52**, 639 (2003); I. Mazin and D. Singh, Phys. Rev. Lett. **79**, 733 (1997).
[15] A. Gukasov *et al.*, Phys. Rev. Lett. **89**, 087202 (2002).
[16] S. C. Wang *et al.*, Phys. Rev. Lett. **93**, 177007 (2004).
[17] V. I. Anisimov *et al.*, Eur. Phys. J. B **25**, 191 (2002).
[18] J. Baier *et al.*, Physica (Amsterdam) **378B**, 497 (2006).
[19] M. Sato *et al.*, J. Phys. Soc. Jpn. **73**, 3418 (2004).